

# Excitons in two-dimensional atomic layer materials from time-dependent density functional theory

Yasumitsu Suzuki<sup>1,\*</sup> and Kazuyuki Watanabe<sup>1</sup>

<sup>1</sup>*Department of Physics, Tokyo University of Science, 1-3 Kagurazaka, Shinjuku-ku, Tokyo 162-8601, Japan*  
(Dated: December 15, 2024)

Time-dependent density functional theory (TDDFT) has been applied to the calculation of absorption spectra for two-dimensional atomic layer materials. We reveal that the character of the first bright exciton state of bi-layer hexagonal boron nitride (h-BN) is dependent on the layer stacking type through the use of many-body perturbation theory (MBPT) calculations, i.e., the electron and hole in the AA' stacking are present in the same layer (intralayer exciton) while the A'B stacking exhibits an interlayer exciton. We demonstrate that the TDDFT approach with the meta-generalized gradient approximation to the exchange-correlation (XC) potential, and the Bootstrap XC kernel can capture the absorption peaks that correspond to these excitons without computationally heavy GW and Bethe-Salpeter equation calculations. We also show that the TDDFT method provides the absorption spectra for mono-layer transition metal dichalcogenides, MoS<sub>2</sub> and MoSe<sub>2</sub>. This study confirms the validity of the TDDFT approach for the first investigation of the optical properties of complex two-dimensional atomic layer materials to which the MBPT calculation can not be readily applied.

## INTRODUCTION

Two-dimensional (2D) atomic layer materials have been gathering more and more attention since an efficient production method for the representative 2D material, graphene, was discovered in 2004 [1]. Many novel properties and physics that appear in these 2D materials due to their distinct electronic structures and the quantum confinement effect have been experimentally and theoretically discovered, such as the quantum Hall effect [2, 3], tightly bound trions [4–6], and the valley degrees of freedom [7–9], just to name a few. Various 2D materials have been synthesized, including metals (e.g., graphene [1]), semiconductors (e.g., mono- and few-layer transition metal dichalcogenides (TMDCs) [10–12]), and insulators (e.g., mono- and few-layer hexagonal boron nitride (h-BN) [13]). These materials have been extensively studied towards their application to nanoscale-thermoelectronic [14–17] and optoelectronic devices [18–20], such as light-harvesting devices [21–24], photo-detectors [25, 26], and light-emitting devices [27–30]. These 2D materials can be combined by van der Waals (vdW) forces as building blocks to produce the vdW heterostructures [31, 32], which can be high-performance optoelectronic devices [33–42]. Atoms or molecules can also be intercalated or adsorbed into these 2D materials as chemical dopants to modify the number of carriers, and to control the absorbance and photoluminescence properties [43–45].

When considering the application of these 2D materials to nano-optoelectronic devices, a first-principles analysis of their optical properties plays a crucial role. If the absorption spectrum (i.e., the imaginary part of macroscopic dielectric function) of the materials could be simulated, then it would be possible to design the best combination of materials that most efficiently ab-

sorb a specific wavelength of light, for example. However, the dielectric screening of the Coulomb interaction in many 2D materials is significantly reduced due to their atomically thin structures when compared to the bulk, and the electron and hole are strongly bound after the absorption of light, i.e., the excitonic effect is enhanced [46]. Consequently, the independent-particle transition picture is considered to break down, and calculation based on Fermi's golden rule, or the random phase approximation (RPA) [47–49] is not adequate to calculate the absorption spectrum of these 2D materials accurately [46]. The method based on the many-body perturbation theory (MBPT) [49, 50], i.e., solving the Bethe-Salpeter equation (BSE) with the GW approximation has generally been used to calculate the electron self-energy (quasiparticle effect) and the excitonic states and the macroscopic dielectric function of these materials [30, 37, 46, 51–61]. However, it is known that both the GW calculation and the BSE calculation require huge computational costs, and thus the application of the MBPT approach to these complex 2D systems, such as heterostructures and molecule-adsorbed systems, remains a challenge, even with the current supercomputers [40, 41, 62–64].

In this study, we investigate the possibility of calculating the absorption spectra of 2D materials using the method based on *time-dependent density functional theory* (TDDFT) [65–67]. TDDFT is a formally exact approach to the time-dependent many-body problem, and in principle it can capture the quasiparticle and excitonic effects, and give the correct spectra [66], as we briefly review these in the next section. The TDDFT approach in the linear response regime can significantly reduce the computational cost compared to the MBPT approach. This is because TDDFT relies on the electron density instead of the Green's function, and only two-point response functions are involved in the formalism,

while the MBPT approach requires the four-point response functions [66, 68–70]. In practice, the exchange-correlation (XC) term that incorporates all many-body effects in the theory must be approximated, and the accuracy of the calculation depends on the quality of the approximation. There has been a long time effort to improve the XC term to capture the excitonic effect in a material [66, 68–81]. Among these efforts, the Bootstrap XC kernel developed by Sharma *et al.* [73, 82] has been reported to be effective to provide a description of the excitonic peaks in the absorption spectra without a requirement for material-dependent parameters. On the other hand, the meta-generalized gradient approximation to the XC potential developed by Tran and Blaha (TB-mBJ potential) [83–85] is known to give correct band gaps of materials, i.e., effectively capture the quasiparticle effect. Nevertheless, the application of the TDDFT approach to 2D materials has been limited to date [86–93], and there have been no studies that applied TDDFT to calculation of the excitonic peaks in the absorption spectra of 2D materials, to the best of our knowledge. Therefore, it is unclear whether the TDDFT approach can describe the absorption peaks that correspond to the interlayer excitons where the electron and hole sit on different layers, which can emerge in multi-layer 2D systems and is important for application in nano-optoelectronics [34, 37, 40–42, 60, 61, 64].

Here we calculate the absorption spectra of 2D materials, mono-layer and bi-layer hexagonal boron nitride (h-BN) and mono-layer TMDCs (MoS<sub>2</sub> and MoSe<sub>2</sub>), using the TDDFT approach with the TB-mBJ potential [83–85] and the Bootstrap kernel [73, 82]. A recent study [94] reported that the character of excitons in bulk h-BN is governed by the layer stacking arrangement. Here we show that the excitons in bi-layer h-BN also have a dependence on the layer stacking by the MBPT calculation, and then demonstrate that the TDDFT approach qualitatively well describes the absorption peaks that correspond to these excitons. We also show that the TDDFT approach well captures the difference in the absorption spectra between mono-layer MoS<sub>2</sub> and MoSe<sub>2</sub> as reported from experimental measurements [95].

## METHODS

### Formalism

In this section we describe the TDDFT approach used in this study. We first review how TDDFT is connected with MBPT and the rigorous form of the XC kernel [66] to remind the reader that TDDFT in principle can describe the excitonic peak energies. We then show those features of the exact XC kernel that are captured by the Bootstrap kernel [73, 82] with the aim to represent the question whether or not these features are effective to

describe the excitonic peaks of 2D materials.

In the linear response TDDFT regime, the response function  $\chi$  is given by the following Dyson-like equation [66] (atomic units are used unless stated otherwise):

$$\chi(1, 2) = \chi_s(1, 2) + \int d3d4 \chi_s(1, 3)[v(3, 4) + f_{xc}(3, 4)]\chi(4, 2), \quad (1)$$

where  $\chi_s$  is the response function of the non-interacting Kohn-Sham system,  $v$  is the bare Coulomb potential, and  $f_{xc}$  is the XC kernel (the numbers represent space-time arguments, e.g.,  $1 = (\mathbf{r}_1, t_1)$ ). The dielectric function is obtained from  $\chi$  through  $\varepsilon^{-1}(\mathbf{q}, \omega) = 1 + v(\mathbf{q})\chi(\mathbf{q}, \omega)$ .

Next we present the connection between TDDFT and MBPT. Defining the proper response function  $\tilde{\chi}$  as  $\chi = \tilde{\chi} + \tilde{\chi}v\chi$  (integration is implied in the appropriate places) [66], the following expression for  $f_{xc}$  is derived:

$$\tilde{\chi}(1, 2) = \chi_s(1, 2) + \int d3d4 \chi_s(1, 3)f_{xc}(3, 4)\tilde{\chi}(4, 2). \quad (2)$$

In MBPT, the propagation of an electron-hole pair is described by the two-particle Green's function, or the four-point polarization function  $L(1, 2, 3, 4)$ , which satisfies the BSE [49, 50]:

$$L(1, 2, 3, 4) = L_0(1, 2, 3, 4) + \int d5d6d7d8 L_0(1, 7, 3, 5)\Gamma(5, 6, 7, 8)L(8, 2, 6, 4). \quad (3)$$

$L_0$  is the non-interacting four-point polarization and  $\Gamma$  is the two-particle scattering amplitude. In the equal time limit,  $L(1, 2, 1, 2)$  reduces to  $\chi(1, 2)$ , and thus the dielectric function that takes account of excitons is obtained once the BSE is solved. Now with the definition of the proper four-point polarization  $\tilde{L}$  as  $L = \tilde{L} + \tilde{L}wL$  and  $\tilde{L} = L_s + L_s\Gamma_{xc}\tilde{L}$  (where  $w(1, 2, 3, 4) = \delta(1, 3)\delta(2, 4)v(1, 2)$ ,  $L_s$  is the four-point polarization of the Kohn-Sham system, and  $\Gamma_{xc}$  is the XC scattering amplitude), the XC kernel that gives the same response function as that from the BSE is given by the following equation [66]:

$$\int d3d4 \chi_s(1, 3)f_{xc}(3, 4)\tilde{\chi}(4, 2) = \int d3d4d5d6 L_s(1, 5, 1, 3)\Gamma_{xc}(3, 4, 5, 6)\tilde{L}(6, 2, 4, 2), \quad (4)$$

which is represented diagrammatically in Fig. 1.

Equation (4) connects the XC kernel in TDDFT with the four-point function in MBPT, and this equation should be the starting point to develop the approximation to the XC kernel. The Bootstrap kernel [73, 82] does capture certain features of the exact XC kernel (4). To observe this, the partition of the XC kernel as a sum

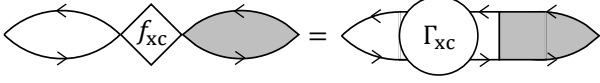


FIG. 1. Diagrammatic representation of Eq. (4) that connects the XC kernel in TDDFT with the four-point function in MBPT.

of a quasiparticle part  $f_{xc}^{qp}$  and an excitonic part  $f_{xc}^{ex}$ ,  $f_{xc} = f_{xc}^{qp} + f_{xc}^{ex}$ , is first introduced with the following relations [96]:

$$\tilde{\chi} = \chi_{qp} + \chi_{qp} f_{xc}^{ex} \tilde{\chi}, \quad (5)$$

$$\chi_{qp} = \chi_s + \chi_s f_{xc}^{qp} \chi_{qp}, \quad (6)$$

where  $\chi_{qp}$  is the response function of non-interacting quasiparticles, i.e.,  $f_{xc}^{qp}$  and  $f_{xc}^{ex}$  bear the quasiparticle and excitonic effect, respectively. The equation that connects  $f_{xc}^{ex}$  with the four-point polarization of the quasiparticle system can now be approximated. Replacement of the scattering amplitude with the screened Coulomb interaction  $W$  [49, 50], and the replacement of  $\tilde{\chi}$  and  $\tilde{L}$  with the corresponding quasiparticle expressions leads to the so-called “nanoquanta” kernel [66, 68–70]:

$$\begin{aligned} & \int d3d4 \chi_{qp}(1, 3) f_{xc}^{ex}(3, 4) \chi_{qp}(4, 2) \\ &= \int d3d4 G_{qp}(1, 3) G_{qp}(4, 1) W(3, 4) G_{qp}(3, 2) G_{qp}(2, 4), \end{aligned} \quad (7)$$

where  $G_{qp}$  is the one-particle Green’s function. The nanoquanta kernel captures the excitonic effect through Eq. (7), but is computationally as expensive as the BSE. One of the important features of the nanoquanta kernel is that it has the form of  $f_{xc}^{ex} \sim \frac{\epsilon^{-1}(0)}{q^2} \alpha$  in the optical limit ( $\mathbf{q} \rightarrow 0$ ) [72]. It has been reported that this  $\mathbf{q}^{-2}$ -divergence [97, 98] in the XC kernel is crucial to take account of the excitonic effect [66, 71, 72, 78].

And from this aspect, the Bootstrap kernel proposed by Sharma *et al.* [73, 82],

$$f_{xc}^{boot} = \frac{\epsilon^{-1}(\mathbf{q}, \omega = 0)}{\chi_s(\mathbf{q}, \omega = 0)}, \quad (8)$$

does capture the feature of the nanoquanta kernel because  $\chi_s(\mathbf{q} \rightarrow 0) = x_0 q^2$  [78, 97, 98], without the requirement of material-dependent parameters or heavy computational cost. In this study we investigate whether these features of the Bootstrap kernel are effective to capture the excitonic effect in 2D materials. We also explore whether the *fully density-functional* approach can be used to predict the absorption spectra of 2D materials. For this purpose,  $\chi_{qp}$  must also be calculated without performing heavy GW calculations [49, 50]. Here we

do not solve Eq. (6) with  $f_{xc}^{qp}$ , but instead  $\chi_{qp}$  is approximated by the Kohn-Sham response function obtained with the TB-mBJ potential functional [83, 84], which is known to yield correct band gaps and thus is expected to take account of the quasiparticle effect.

## Computational details

The TDDFT and MBPT calculations have been performed using the full-potential linearized augmented plane wave codes `Elk` [99] and `exciting` [100–102], respectively. In the ground-state calculation and the TDDFT calculation, a basis-set cutoff  $R_{MT} G_{max} = 7$  is used, while in the BSE calculation,  $R_{MT} G_{max} = 6$  is used. A muffin-tin radius  $R_{MT} = 1.3$  bohr is adopted for all atomic species involved in the simulation. In the MBPT calculation, the ground-state electron densities are computed in the framework of density functional theory using the PBE XC potential functional [103]. Sampling of the Brillouin zone is  $18 \times 18 \times 1$   $\mathbf{k}$ -points for the ground-state calculation,  $10 \times 10 \times 1$  shifted  $\mathbf{k}$ -points for calculation of the quasiparticle correction to the Kohn-Sham eigenvalue within the  $G_0W_0$  approximation, and  $24 \times 24 \times 1$  shifted  $\mathbf{k}$ -points for the BSE calculation. 60 empty states are included in all  $G_0W_0$  and BSE calculations. In the construction of the BSE Hamiltonian, two occupied and two unoccupied bands are considered for mono-layer h-BN, and four occupied and four unoccupied bands are considered for bi-layer h-BN. In the TDDFT calculation, the TB-mBJ potential functional [83] is used to obtain the approximate quasiparticle response function  $\chi_{qp}$ , as explained in the previous section, and the Bootstrap kernel [73] is used to solve the Dyson-like equation (1). Brillouin zone sampling is  $24 \times 24 \times 1$   $\mathbf{k}$ -points. These parameters ensure the results that are sufficiently converged for our discussion below.

## RESULTS

### Excitons in bi-layer h-BN from the MBPT approach

We first discuss the absorption spectra of bi-layer h-BN calculated with the MBPT approach. Both bulk and a few-layer h-BNs are insulators that exhibit large excitonic peaks in the absorption spectra [57–61, 94, 104, 105]. A recent study [94] has reported that the characteristics of excitons in bulk h-BN are largely influenced by the layer stacking; for example, the 3D exciton, where the electron distribution overlaps with the hole distribution and also extends to the adjacent layers, appears only in the layer configuration where inversion symmetry is present. The dependence of the exciton characteristics on the layer stacking arises from the difference in

the electronic structure of the bands that contribute to the excitonic states [94].

In this subsection, we investigate whether the dependence of excitons on the layer stacking appear also in bi-layer h-BN using the MBPT calculation, and those characteristics of excitons that dominate the onset of absorption. Our purpose in this study is to confirm whether or not the TDDFT method can be used to simulate the absorption spectra of 2D materials, in particular whether it can describe the first absorption peaks that may correspond to interlayer or intralayer excitons. Therefore, we must first clarify in which layer configuration the interlayer and intralayer excitons appear as the first peak in the absorption spectra of bi-layer h-BN.

To this end, we focus on two types of layer stacking: AA' and A'B configurations. In the AA' stacking configuration, B and N atoms of the first layer lie on top of different atoms in the second layer, while in A'B stacking, the N atoms occupy the hollow position and the B atoms are aligned on top of each other [94]. These two configurations are selected because they are reported to exhibit totally different excitonic characters in bulk-hBN [94], and it is expected that the difference between these configurations will also appear in the bi-layer case.

Figure 2(a) shows the unit cells (repeated four times for the sake of clarity) for AA' stacking (left) and A'B stacking (right) bi-layer h-BN. We set the in-plane lattice parameter as 2.50 Å for both stacking arrangements, while the interlayer distances are set as 3.30 Å for AA' stacking and as 3.24 Å for A'B stacking, so that these parameters are the same as those of their bulk counterparts [94]. To model the 2D bi-layer system, the unit cell must have a vacuum region in the out-of-plane direction (c-direction in Fig. 2(a)) that should be sufficiently large to avoid interaction between replica images due to the periodic boundary conditions and to correctly take account of the reduction of screening. We set the length of the vacuum region as 18 bohr ( $\approx 9.5$  Å) for both stacking arrangements because in the previous study on monolayer h-BN [57], it was demonstrated that the impact of the vacuum region length on the absorption spectrum starts to converge when the length exceeds approximately 18 bohr. Thus, we consider that 18 bohr vacuum region is sufficient for at least a primary discussion that focuses on the difference in the characteristics of excitonic peaks between different stacking systems.

Quasiparticle band structures calculated for these two systems by the MBPT approach (with  $G_0W_0$  approximation) are shown in Fig. 2(b). The overall band structures are similar between AA' (red) and A'B (blue) stacking. However, the two lowest conduction bands are degenerate at the K point in the Brillouin zone for AA' stacking, while they are energetically split for A'B stacking. Similar degeneracy and splitting of the bands were reported for bulk h-BN case (along the K-H path) [94, 104, 106, 107], and the mechanism should also be the same;

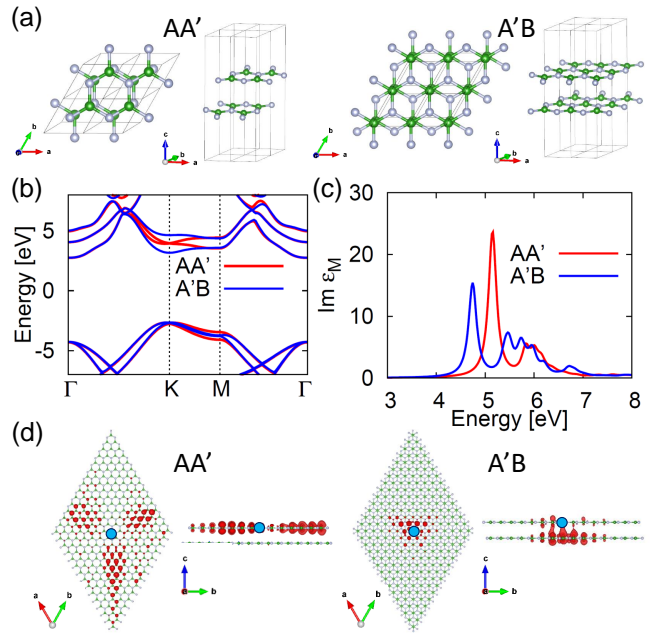


FIG. 2. (a) Two types of layer-stacking configuration that were examined for bi-layer h-BN: AA' stacking (left) and A'B stacking (right). For the sake of clarity, the figures show the unit cell repeated four times. B atoms are green and N atoms are gray. (b) Quasiparticle band structures of two considered stacking arrangements (AA': red and A'B: blue). (c) Optical absorption spectra for the two considered stacking arrangements (AA': red and A'B: blue) calculated by the MBPT ( $G_0W_0$ +BSE) approach. (d) Real-space distribution of the electron component (red isosurface) of the exciton wavefunction that gives rise to the first peak of the absorption spectrum (left: AA' stacking, right: A'B stacking). Isovalues of 12% of the maximum values are adopted. The position of the fixed hole is indicated by a blue dot.

the degeneracy of the two lowest conduction bands and the degeneracy of the two highest valence bands occur when the atoms of the same species do not lie on top of each other (such as AA' stacking), while they are split when they are on top of each other (such as A'B stacking) because of the weak electrostatic interaction between atoms of the same species.

The optical absorption spectra (the imaginary part of the macroscopic dielectric function) of these two systems calculated by solving the BSE are presented in Fig. 2(c) to show how the differences in the electronic states result in the excitonic peaks. It is evident that there is a considerable difference between the two absorption spectra, i.e., the first intense excitonic peak appears at a lower energy in the spectrum for A'B stacking (blue) than that for AA' stacking (red); the onset of absorption is red-shifted with A'B stacking. Similar differences in the absorption spectra between AA' and A'B stacking have been reported for bulk h-BN [94], and here

we have shown that there is also dependence of the absorption spectra on the layer stacking in 2D bi-layer h-BN.

To understand the difference in the excitonic characteristics between these two different layer-stacking bi-layer h-BNs, the real-space distribution of the electron component of the exciton wavefunction that gives rise to the first peak of each absorption spectrum is plotted in Fig. 2 (d) as red isosurfaces (isovalues of 12% of the maximum values are adopted). The position of the fixed hole is indicated by a blue dot in the figure. For AA' stacking (left), it is clear that the electron and hole exist in the same layer, i.e., the intralayer exciton is responsible for the first absorption peak, while for the A'B exciton case (right), a major portion of the electron and hole are located on different layers, and thus it can be regarded as an interlayer exciton. Therefore, these two different layer-stacking bi-layer h-BNs exhibit different absorption peaks that have different excitonic characteristics. Bi-layer h-BNs thus represent ideal systems to investigate the effectiveness of the TDDFT approach to the study of the optical properties of 2D materials, which will be clarified by TDDFT calculations for these two different excitonic peaks.

#### TDDFT calculation of the absorption spectra of 2D materials

The results of TDDFT calculations of the absorption spectra of 2D materials are presented here. Before the results for the bi-layer h-BNs are discussed, we first present the results for mono-layer h-BN, for which many reference data are available from previous studies [57–59].

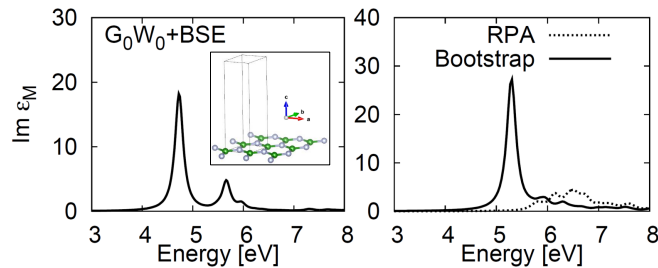


FIG. 3. Absorption spectra for mono-layer h-BN calculated by the MBPT approach (left panel) and the TDDFT approach (right panel, solid line). The RPA result is also shown as a dotted line in the inset of the left panel. The unit cell is shown in the inset of the left panel.

The left panel of Fig. 3 shows the absorption spectrum of mono-layer h-BN calculated by the MBPT approach ( $G_0W_0+BSE$ ) together with the unit cell employed (inset). The length of the vacuum region is again set as

18 bohr. The spectrum shows two characteristic peaks. These structures are in good agreement with those calculated in previous studies [57–59]. A slight red-shift of the peaks is evident in the spectrum compared to those from previous reports [57–59], which could be attributed to the small vacuum region used in the present calculation.

The spectrum calculated by the TDDFT approach (equipped with the Bootstrap XC kernel and TB-mBJ XC potential) is plotted as a solid line in the right panel of Fig. 3. The result of RPA calculation (i.e., setting  $f_{xc}^{ex} = 0$  in the TDDFT equations) is also plotted as a dotted line in the right panel. A comparison of these spectra indicates that the spectrum calculated by the TDDFT approach is qualitatively in good agreement with that from the MBPT calculation, i.e., the TDDFT spectrum also shows the intense first peak and the relatively weak second peak, which are completely missed in the RPA result. The positions of these peaks in terms of energy are also in agreement with those in the MBPT result, although the TDDFT peaks are slightly blue-shifted. Therefore, the present strategy to model  $\chi_{qp}$  using the TB-mBJ potential and incorporate the excitonic effect through the use of the Bootstrap kernel were effective to simulate the excitonic peaks in the absorption spectrum of 2D mono-layer h-BN.

Having demonstrated a successful example of the TDDFT approach to simulate the absorption spectrum of mono-layer h-BN, we now present the results for the bi-layer h-BNs. The optical absorption spectra for the

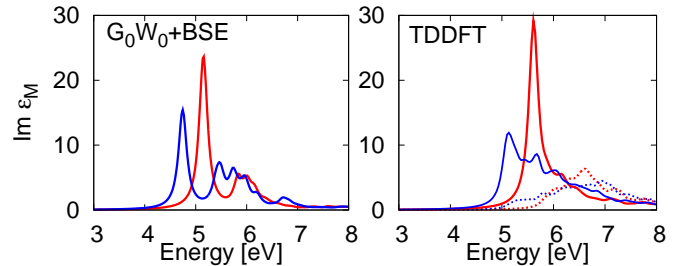


FIG. 4. Absorption spectra for two different layer-stacking bi-layer h-BNs calculated by the MBPT approach (left panel, the same as Fig. 2(c)) and the TDDFT approach (right panel, solid lines). Red lines are for AA' stacking and blue lines are for A'B stacking. The RPA results are also shown as a dotted line in the right panel.

AA' (red line) and A'B (blue line) stacking bi-layer h-BNs calculated by the TDDFT approach are shown as solid lines in the right panel of Fig. 4. For comparison, the MBPT results (Fig. 2 (c)) are again shown in the left panel. The RPA results are also plotted as dotted lines in the right panel. From a comparison of these results, it is evident that the TDDFT approach with the Bootstrap kernel does qualitatively well describe the difference in the excitonic peaks between the AA' and A'B stacking

arrangements, i.e., the difference between the position and intensity of the first peak for AA' stacking (which corresponds to the intralayer exciton) and those of the first peak for A'B stacking (which corresponds to the interlayer exciton). The other excitonic peaks shown in the MBPT results are also qualitatively captured by the TDDFT calculations. On the other hand, the RPA calculation does not describe the peak structures correctly. These results indicate that the TDDFT approach with the Bootstrap kernel and TB-mBJ potential are useful to simulate the difference in the absorption spectra between the different layer-stacking bi-layer h-BNs. The calculated spectra can be used for qualitative discussions, for example, prediction of the difference in the onset of absorption. It is also demonstrated that the TDDFT approach can capture the excitonic peaks that correspond to the interlayer exciton, which is important when considering the application to photovoltaics, for example.

Finally, we present the results of TDDFT calculations for other 2D materials, i.e., mono-layer MoS<sub>2</sub> and mono-layer MoSe<sub>2</sub>, to show the validity of the TDDFT approach to the study of the optical properties of general 2D materials. The few-layer TMDCs have been considerably remarked as post-graphene materials and the building blocks of vdW heterostructures [4–6, 10–12, 18–29, 33–38, 40, 42–45, 95], and their application to nano-optoelectronic devices is highly expected. The absorp-

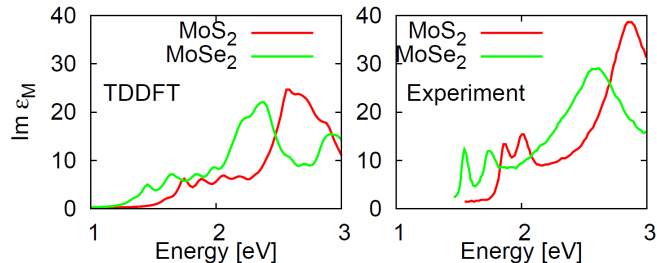


FIG. 5. Absorption spectra of mono-layer MoS<sub>2</sub> (red) and mono-layer MoSe<sub>2</sub> (green) calculated by the TDDFT approach (left panel). The right panel shows the experimental results [95].

tion spectra of mono-layer MoS<sub>2</sub> (red) and mono-layer MoSe<sub>2</sub> (green) calculated by the TDDFT approach are shown in the left panel of Fig. 5. It should be noted that the spin-orbit coupling is explicitly taken into account in these calculations because the heavy element molybdenum is included in the system. As a result the TB-mBJ potential functional cannot be used [83, 84, 99]; therefore, the LDA XC potential [108] is used for these calculations and only the effect of the Bootstrap kernel is studied. The right panel of Fig. 5 shows the experimental results [95]. A comparison of the left and right panels indicates that the TDDFT approach again captures the overall features of the absorption peaks. The excessive splitting of the excitonic peaks is attributed to

the spin-orbit coupling, which can be eliminated by taking account of the lifetime effect due to electron-phonon coupling [53]. It should also be noted that in these systems (mono-layer MoS<sub>2</sub> and mono-layer MoSe<sub>2</sub>), the RPA calculation (not shown here) also gives similar peak structures as the experimental measurement, although the peak intensities are considerably underestimated. Therefore, these results for mono-layer TMDCs also support the usefulness of the TDDFT approach for the study of the optical properties of 2D materials.

## SUMMARY

We have applied the TDDFT approach with the TB-mBJ potential functional and the Bootstrap kernel to the calculation of absorption spectra for 2D atomic layer materials, mono-layer h-BN, bi-layer h-BNs, and mono-layer MoS<sub>2</sub> and MoSe<sub>2</sub>. The TDDFT approach well captures the excitonic peaks of these materials. In particular, for the bi-layer h-BNs, the TDDFT approach can describe the excitonic peaks that correspond to the interlayer exciton and intralayer exciton, and captures the difference in the absorption spectra between the different layer stacking arrangements. These results indicate that the TDDFT approach with the Bootstrap kernel and TB-mBJ potential successfully captures the features of the exact XC kernel (described in the **Formalism section** above) that are essential to describe the quasiparticle and excitonic effects in these 2D materials.

This study demonstrates the validity of the TDDFT approach for the primary study of the optical properties of 2D materials. The TDDFT approach has advantages over the MBPT approach in terms of computational efficiency. Improving the XC terms will improve the accuracy of the TDDFT approach, so that it will become one of the key simulation tools in the development of 2D material science.

Y. S. is supported by JSPS KAKENHI Grant No. JP16K17768 and JP19K03675. K. W. is supported by JSPS KAKENHI Grant No. JP16K05483. Part of the computations were performed on the supercomputers of the Institute for Solid State Physics, The University of Tokyo.

\* yasumitsu.suzuki@rs.tus.ac.jp

- [1] K. S. Novoselov, A. K. Geim, S. V. Morozov, D. Jiang, Y. Zhang, S. V. Dubonos, I. V. Grigorieva, and A. A. Firsov, *Science* **306**, 666 (2004).
- [2] K. S. Novoselov, A. K. Geim, S. V. Morozov, D. Jiang, M. I. Katsnelson, I. V. Grigorieva, S. V. Dubonos, and A. A. Firsov, *Nature* **438**, 197 (2005).
- [3] Y. Zhang, Y.-W. Tan, H. L. Stormer, and P. Kim, *Nature* **438**, 201 (2005).

- [4] K. F. Mak, K. He, C. Lee, G. H. Lee, J. Hone, T. F. Heinz, and J. Shan, *Nat. Mater.* **12**, 207 (2013).
- [5] G. Plechinger, P. Nagler, A. Arora, R. Schmidt, A. Chernikov, A. G. del Águila, P. C. M. Christianen, R. Bratschitsch, C. Schüller, and T. Korn, *Nat. Commun.* **7**, 12715 (2016).
- [6] A. Ramirez-Torres, V. Turkowski, and T. S. Rahman, *Phys. Rev. B* **90**, 085419 (2014).
- [7] K. Behnia, *Nat. Nanotechnol.* **7**, 488 (2012).
- [8] J. R. Schaibley, H. Yu, G. Clark, P. Rivera, J. S. Ross, K. L. Seyler, W. Yao, and X. Xu, *Nat. Rev. Mater.* **1**, 16055 (2016).
- [9] Y. Miyauchi, S. Konabe, F. Wang, W. Zhang, A. Hwang, Y. Hasegawa, L. Zhou, S. Mouri, M. Toh, G. Eda, and K. Matsuda, *Nat. Commun.* **9**, 2598 (2018).
- [10] A. Splendiani, L. Sun, Y. Zhang, T. Li, J. Kim, C.-Y. Chim, G. Galli, and F. Wang, *Nano Lett.* **10**, 1271 (2010).
- [11] B. Radisavljevic, A. Radenovi, J. Brivio, V. Giacometti, and A. Kis, *Nat. Nanotechnol.* **6**, 147 (2011).
- [12] M. Chhowalla *et al.*, *Nat. Chem.* **5**, 263 (2013).
- [13] Y. Stehle, H. M. Meyer III, R. R. Unocic, M. Kidder, G. Polizos, P. G. Datskos, R. Jackson, S. N. Smirnov, and I. V. Vlassioug, *Chem. Mater.* **27**, 8041 (2015).
- [14] J. Wu, H. Schmidt, K. K. Amara, X. Xu, G. Eda, and B. Özyilmaz, *Nano Lett.* **14**, 2730 (2014).
- [15] K.-X. Chen, S.-S. Lyu, X.-M. Wang, Y.-X. Fu, Y. Heng, and D.-C. Mo, *J. Phys. Chem. C* **121**, 13035 (2017).
- [16] Ch. Adessi, S. Thebaud, R. Bouzerar, and G. Bouzerar, *J. Phys. Chem. C* **121**, 12577 (2017).
- [17] L. Zhu, F. Zou, G. Gao, and K. Yao, *Sci. Rep.* **7**, 497 (2017).
- [18] Q. H. Wang, K. Kalantar-Zadeh, A. Kis, J. N. Coleman, and M. S. Strano, *Nat. Nanotechnol.* **7**, 699 (2012).
- [19] K. F. Mak and J. Shan, *Nat. Photonics* **10**, 216 (2016).
- [20] D. Jariwala, V. K. Sangwan, L. J. Lauhon, T. J. Marks, and M. C. Hersam, *ACS Nano* **8**, 1102 (2014).
- [21] M.-L. Tsai, S.-H. Su, J.-K. Chang, D.-S. Tsai, C.-H. Chen, C.-I. Wu, L.-J. Li, L.-J. Chen, and J.-H. He, *ACS Nano* **8**, 8317 (2014).
- [22] M. Bernardi, M. Palummo, and J. C. Grossman, *Nano Lett.* **13**, 3664 (2013).
- [23] L. Britnell, R. M. Ribeiro, A. Eckmann, R. Jalil, B. D. Belle, A. Mishchenko, Y.-J. Kim, R. V. Gorbachev, T. Georgiou, S. V. Morozov, A. N. Grigorenko, A. K. Geim, C. Casiraghi, A. H. Castro Neto, and K. S. Novoselov, *Science* **340**, 1311 (2013).
- [24] O. Lopez-Sanchez, E. Alarcon Llado, V. Koman, A. Fontcubertai Morral, A. Radenovic, and A. Kis, *ACS Nano* **8**, 3042 (2014).
- [25] H. S. Lee, S. W. Min, Y. G. Chang, M. K. Park, T. Nam, H. Kim, J. H. Kim, S. Ryu, and S. Im, *Nano Lett.* **12**, 3695 (2012).
- [26] J. Xia, X. Huang, L.-Z. Liu, M. Wang, L. Wang, B. Huang, D.-D. Zhu, L. J.-J., C.-Z. Gu, and X.-M. Meng, *Nanoscale* **6**, 8949 (2014).
- [27] R. S. Sundaram, M. Engel, A. Lombardo, R. Krupke, A. C. Ferrari, Ph. Avouris, and M. Steiner, *Nano Lett.* **13**, 1416 (2013).
- [28] Y. J. Zhang, T. Oka, R. Suzuki, J. T. Ye, and Y. Iwasa, *Science* **344**, 725 (2014).
- [29] J. S. Ross, P. Klement, A. M. Jones, N. J. Ghimire, J. Yan, D. Mandrus, T. Taniguchi, K. Watanabe, K. Kitamura, W. Yao, D. H. Cobden, and X. Xu, *Nat. Nanotechnol.* **9**, 268 (2014).
- [30] R. Bourrellier, M. Amato, L. Henrique, G. Tizei, C. Giorgetti, A. Gloter, M. I. Heggie, K. March, O. Stéphan, L. Reining, M. Kociak, and A. Zobelli, *ACS Photonics* **1**, 857 (2014).
- [31] A. K. Geim and I. V. Grigorieva, *Nature* **499**, 419 (2013).
- [32] J. Wang, F. Ma, and M. Sun, *RSC Adv.* **7**, 16801 (2017).
- [33] D. Kozawa, R. Kumar, A. Carvalho, K. K. Amara, W. Zhao, S. Wang, M. Toh, R. M. Ribeiro, A. H. Castro Neto, K. Matsuda, and G. Eda, *Nat. Commun.* **5**, 4543 (2014).
- [34] S. Mouri, W. Zhang, D. Kozawa, Y. Miyauchi, G. Eda, and K. Matsuda, *Nanoscale* **9**, 6674 (2017).
- [35] K. S. Novoselov, A. Mishchenko, A. Carvalho, and A. H. Castro Neto, *Science* **353**, aac9439 (2016).
- [36] D. Jariwala, T. J. Marks, and M. C. Hersam, *Nat. Mater.* **16**, 170 (2017).
- [37] M. Okada, A. Kutana, Y. Kureishi, Y. Kobayashi, Y. Saito, T. Saito, K. Watanabe, T. Taniguchi, S. Gupta, Y. Miyata, B. I. Yakobson, H. Shinohara, and R. Kitaura, *ACS Nano* **12**, 2498 (2018).
- [38] A. Nourbakhsh, A. Zubair, M. S. Dresselhaus, and T. Palacios, *Nano Lett.* **16**, 1359 (2016).
- [39] T. Hu and J. Hong, *ACS Appl. Mater. Interfaces* **7**, 23489 (2015).
- [40] S. Latini, K. T. Winther, T. Olsen, and K. S. Thygesen, *Nano Lett.* **17**, 938 (2017).
- [41] Y. Chen and S. Y. Quek, *2D Mater.* **5**, 045031 (2018).
- [42] P. K. Nayak, Y. Horbatenko, S. Ahn, G. Kim, J.-U. Lee, K. Y. Ma, A.-R. Jang, H. Lim, D. Kim, S. Ryu, H. Cheong, N. Park, and H. S. Shin, *ACS Nano* **11**, 4041 (2017).
- [43] S. Mouri, Y. Miyauchi, and K. Matsuda, *Nano Lett.* **13**, 5944 (2013).
- [44] S. Mouri, Y. Miyauchi, and K. Matsuda, *Appl. Phys. Express* **9**, 055202 (2016).
- [45] M. Amani, D.-H. Lien, D. Kiriya, J. Xiao, A. Azcatl, J. Noh, S. R. Madhupathy, R. Addou, S. KC, M. Dubey, K. Cho, R. M. Wallace, S.-C. Lee, J.-H. He, J. W. Ager III, X. Zhang, E. Yablonovitch, and A. Javey, *Science* **350**, 1065 (2015).
- [46] H. Sahin, E. Torun, C. Bacaksiz, S. Horzum, J. Kang, R. T. Senger, and F. M. Peeters, *WIREs Comput. Mol. Sci.* **6**, 351 (2016).
- [47] S. L. Adler, *Phys. Rev.* **126**, 413 (1962).
- [48] N. Wisser, *Phys. Rev.* **129**, 62 (1963).
- [49] G. Onida, L. Reining, and A. Rubio, *Rev. Mod. Phys.* **74**, 601 (2002).
- [50] F. Bechstedt, *Many-Body Approach to Electronic Excitations* (Springer, 2015).
- [51] L. Yang, J. Deslippe, C.-H. Park, M. L. Cohen, and S. G. Louie, *Phys. Rev. Lett.* **103**, 186802 (2009).
- [52] A. Ramasubramaniam, *Phys. Rev. B* **86**, 115409 (2012).
- [53] D. Y. Qiu, F. H. da Jornada, and S. G. Louie, *Phys. Rev. Lett.* **111**, 216805 (2013).
- [54] A. Molina-Sánchez, D. Sangalli, K. Hummer, A. Marini, and L. Wirtz, *Phys. Rev. B* **88**, 045412 (2013).
- [55] H. Shi, H. Pan, Y.-W. Zhang, and B. I. Yakobson, *Phys. Rev. B* **87**, 155304 (2013).
- [56] D. Azhikodan, T. Nautiyal, S. Shallcross, and S. Sharma, *Sci. Rep.* **6**, 37075 (2016).
- [57] L. Wirtz, A. Marini, and A. Rubio, *Phys. Rev. Lett.* **96**, 126104 (2006).
- [58] P. Cudazzo, L. Sponza, C. Giorgetti, L. Reining, F. Sottile, and M. Gatti, *Phys. Rev. Lett.* **116**, 066803 (2016).

- [59] F. Ferreira, A. J. Chaves, N. M. R. Peres, and R. M. Ribeiro, *J. Opt. Soc. Am. B* **36**, 674 (2019).
- [60] M. Ashhadi and S. A. Ketabi, *Solid State Commun.* **187**, 1 (2014).
- [61] F. Paleari, T. Galvani, H. Amara, F. Ducastelle, A. Molina-Sánchez, and L. Wirtz, *2D Mater* **5**, 045017 (2018).
- [62] J. Yan, K. W. Jacobsen, and K. S. Thygesen, *Phys. Rev. B* **86**, 045208 (2012).
- [63] H.-P. Komsa and A. V. Krasheninnikov, *Phys. Rev. B* **88**, 085318 (2013).
- [64] R. Gillen and J. Maultzsch, *Phys. Rev. B* **97**, 165306 (2018).
- [65] E. Runge and E. K. U. Gross, *Phys. Rev. Lett.* **52**, 997 (1984).
- [66] C. A. Ullrich, *Time-Dependent Density-Functional Theory: Concepts and Applications* (Oxford University Press, 2012).
- [67] N. T. Maitra, *J. Chem. Phys.* **144**, 220901 (2016).
- [68] L. Reining, V. Olevano, A. Rubio, and G. Onida, *Phys. Rev. Lett.* **88**, 066404 (2002).
- [69] F. Sottile, V. Olevano, and L. Reining, *Phys. Rev. Lett.* **91**, 056402 (2003).
- [70] A. Marini, R. Del Sole, and A. Rubio, *Phys. Rev. Lett.* **91**, 256402 (2003).
- [71] S. Botti, F. Sottile, N. Vast, V. Olevano, L. Reining, H.-C. Weissker, A. Rubio, G. Onida, R. Del Sole, and R. W. Godby, *Phys. Rev. B* **69**, 155112 (2004).
- [72] S. Botti, A. Fourreau, F. Nguyen, Y.-O. Renault, F. Sottile, and L. Reining, *Phys. Rev. B* **72**, 125203 (2005).
- [73] S. Sharma, J. K. Dewhurst, A. Sanna, and E. K. U. Gross, *Phys. Rev. Lett.* **107**, 186401 (2011).
- [74] Z.-H. Yang, Y. Li, and C. A. Ullrich, *J. Chem. Phys.* **137**, 014513 (2012).
- [75] Z.-H. Yang and C. A. Ullrich, *Phys. Rev. B* **87**, 195204 (2013).
- [76] S. Rigamonti, S. Botti, V. Veniard, C. Draxl, L. Reining, and F. Sottile, *Phys. Rev. Lett.* **114**, 146402 (2015).
- [77] Z.-H. Yang, F. Sottile, and C. A. Ullrich, *Phys. Rev. B* **92**, 035202 (2015).
- [78] Y.-M. Byun and C. A. Ullrich, *Phys. Rev. B* **95**, 205136 (2017).
- [79] Y.-M. Byun and C. A. Ullrich, *Computation* **5**, 9 (2017).
- [80] A. V. Terentjev, L. A. Constantin, and J. M. Pitarke, *Phys. Rev. B* **98**, 085123 (2018).
- [81] N. Singh, P. Elliott, T. Nautiyal, J. K. Dewhurst, and S. Sharma, *Phys. Rev. B* **99**, 035151 (2019).
- [82] S. Sharma, J. K. Dewhurst, S. Shallcross, G. K. Madjarova, and E. K. U. Gross, *J. Chem. Theory Comput.* **11**, 1710 (2015).
- [83] F. Tran and P. Blaha, *Phys. Rev. Lett.* **102**, 226401 (2009).
- [84] D. J. Singh, *Phys. Rev. B* **82**, 205102 (2010).
- [85] S. A. Sato, Y. Taniguchi, Y. Shinohara, and K. Yabana, *J. Chem. Phys.* **143**, 224116 (2015).
- [86] P. Li, X. Ren, and L. He, *Phys. Rev. B* **96**, 165417 (2017).
- [87] V. Turkowski, N. U. Din, and T. S. Rahman, *Computation* **5**, 39 (2017).
- [88] S. Yamada, M. Noda, K. Nobusada, and K. Yabana, *Phys. Rev. B* **98**, 245147 (2018).
- [89] Y. Miyamoto and A. Rubio, *J. Phys. Soc. Jpn.* **87**, 041016 (2018).
- [90] U. De Giovannini, H. Hübener, and A. Rubio, *J. Chem. Theory Comput.* **13**, 265 (2017).
- [91] S. A. Sato, H. Hübener, U. De Giovannini, and A. Rubio, *Appl. Sci.* **8**, 1777 (2018).
- [92] Z. Wang, S.-S. Li, and L.-W. Wang, *Phys. Rev. Lett.* **114**, 063004 (2015).
- [93] Y. Ueda, Y. Suzuki, and K. Watanabe, *Phys. Rev. B* **97**, 075406 (2018).
- [94] W. Aggoune, C. Cocchi, D. Nabok, K. Rezouali, M. A. Belkhir, and C. Draxl, *Phys. Rev. B* **97**, 241114(R) (2018).
- [95] Y. Li, A. Chernikov, X. Zhang, A. Rigosi, H. M. Hill, A. M. van der Zande, D. A. Chenet, E.-M. Shih, J. Hone, and T. F. Heinz, *Phys. Rev. B* **90**, 205422 (2014).
- [96] R. Stubner, I. V. Tokatly, and O. Pankratov, *Phys. Rev. B* **70**, 245119 (2004).
- [97] Ph. Ghosez, X. Gonze, and R. W. Godby, *Phys. Rev. B* **56**, 12811 (1997).
- [98] Y.-H. Kim and A. G'orling, *Phys. Rev. B* **66**, 035114 (2002).
- [99] *The Elk FP-LAPW Code* (accessed 2017), <https://elk.sourceforge.net>.
- [100] A. Gulans, S. Kontur, C. Meisenbichler, D. Nabok, P. Pavone, S. Rigamonti, S. Sagmeister, U. Werner, and C. Draxl, *J. Phys.: Condens. Matter* **26**, 363202 (2014).
- [101] S. Sagmeister and C. Draxl, *Phys. Chem. Chem. Phys.* **11**, 4451 (2009).
- [102] D. Nabok, A. Gulans, and C. Draxl, *Phys. Rev. B* **94**, 035118 (2016).
- [103] J. P. Perdew, K. Burke, and M. Ernzerhof, *Phys. Rev. Lett.* **77**, 3865 (1996).
- [104] B. Arnaud, S. Lebegue, P. Rabiller, and M. Alouani, *Phys. Rev. Lett.* **96**, 026402 (2006).
- [105] L. Wirtz, A. Marini, M. Gr'uning, C. Attaccalite, G. Kresse, and A. Rubio, *Phys. Rev. Lett.* **100**, 189701 (2008).
- [106] L. Liu, Y. P. Feng, and Z. X. Shen, *Phys. Rev. B* **68**, 104102 (2003).
- [107] S.-P. Gao, *Solid State Commun.* **152**, 1817 (2012).
- [108] J. P. Perdew and Y. Wang, *Phys. Rev. B* **45**, 13244 (1992).